Cyano-Bridged Re_6Q_8 (Q = S, Se) Cluster-Cobalt(II) Framework Materials: Versatile Solid Chemical Sensors

Laurance G. Beauvais, Matthew P. Shores, and Jeffrey R. Long*

Contribution from the Department of Chemistry, University of California, Berkeley, California 94720-1460

Received November 30, 1999

Abstract: Face-capped octahedral clusters of the type $[Re_6Q_8(CN)_6]^{4-}$ (Q = S, Se) are used to space apart partially hydrated Co^{2+} ions in extended solid frameworks, creating porous materials that display dramatic color changes upon exposure to certain organic solvents. The clusters react with cobaltous ions in aqueous solution to precipitate the new solid phases $[Co_2(H_2O)_4][Re_6S_8(CN)_6]\cdot 10H_2O$ (**1**), $Cs_2[Co(H_2O)_2][Re_6S_8(CN)_6]\cdot 2H_2O$ (**2**), and $[Co(H_2O)_3]_4[Co_2(H_2O)_4][Re_6Se_8(CN)_6]_3\cdot 44H_2O$ (**3**). The structures of **1**·$2H_2O$ and **3** were determined by single-crystal X-ray analysis. The former consists of an expanded Prussian blue type framework with $[Re_6S_8]^{2+}$ and $[Co_2(\mu\text{-}OH_2)_2]^{4+}$ cluster cores occupying alternate metal ion sites, and features cubelike cages enclosing water-filled cavities approximately 258 Å^3 in volume. The latter structure exhibits a network of Co^{2+} ions and $[Co_2(\mu\text{-}OH_2)_2]^{4+}$ cores connected through $[Re_6Se_8(CN)_6]^{4-}$ clusters, defining an array of one-dimensional channels with minimum internal diameters of 4.8 Å. A Rietveld refinement against X-ray powder diffraction data established compound **2** as isostructural to an analogous Fe-containing phase with a two-dimensional framework reminiscent of the Hoffman clathrates. Thermogravimetric analyses show that all three compounds are fully dehydrated by ca. 100 °C, with no further significant loss of mass below 500 °C. Upon exposure to diethyl ether vapor, the color of compounds **1** and **3** immediately changes from orange to an intense blue-violet or blue; other polar solvents induce somewhat different colors. These (reversible) changes are associated with the emergence of an envelope of new absorption features at wavelengths between 500 and 650 nm, and the magnitude of the response to a solvent can be estimated by measuring the relative intensity of a band with a maximum near 600 nm. We propose that the vapochromic response is due to solvent molecules entering the pores of the solid, where they disrupt the hydrogen-bonded water network, prompting the release of bound water from the $[Co_2(H_2O)_4]^{4+}$ clusters and conversion of their Co centers from octahedral to tetrahedral coordination. Significantly, this process does not destroy the three-dimensional connectivity in either structure, but rather creates a much more flexible framework that can expand to accommodate the incoming solvent molecules. Spectroscopic and magnetic data confirm the change in coordination geometry, and the trends in solvent responses (e.g., methanol < ethanol < *n*-propanol < *i*-propanol) are consistent with a decreased ability to support the bridging water ligands of the clusters as steric bulk increases. Size-selective sensing is demonstrated with methyl *tert*-butyl ether, which causes a color change in compound **3**, but not in compound **1**. X-ray powder diffraction experiments indicate that the vapochromic response in both compounds is affiliated with a reversible change in the bulk crystal structure of the material. Variable-temperature magnetic susceptibility data for compound **1** suggest a weak antiferromagnetic coupling interaction between the water-bridged Co^{2+} ions of the dinuclear cluster units. Finally, a simple chemical sensing device employing these solids is described, along with some properties relevant to its function.

Introduction

The prospect of obtaining solid materials with tailored properties and reactivity has aroused interest in solution-based methods for their synthesis, whereby soluble molecular components can be organized into extended solid frameworks.[1] Often the goal in such research is to design a porous material that can act as a catalyst[2] or molecular sieve[3−5] by choosing appropriate molecular building blocks. However, the most widespread success with this technique has perhaps been achieved in the synthesis of magnetic materials composed of exchange-coupled paramagnetic transition-metal centers.[6] The versatility of the

(1) (a) Hoskins, B. F.; Robson, R. *J. Am. Chem. Soc.* **1990**, *112*, 1546. (b) Zaworotko, M. J. *Chem. Soc. Rev.* **1994**, 283. (c) Moore, J. S.; Lee, S. *Chem. Ind.* **1994**, 556. (d) Ward, M. D. *Nature* **1995**, *374*, 764. (e) Bowes, C. L.; Ozin, G. A. *Adv. Mater.* **1996**, *8*, 13 and references therein.

(2) Fujita, M.; Kwon, Y. J.; Washizu, S.; Ogura, K. *J. Am. Chem. Soc.* **1994**, *116*, 1151.

(3) (a) Boxhoorn, G.; Moolhuysen, J.; Coolegem, J. G. F.; van Santen, R. A. *J. Chem. Soc., Chem. Commun.* **1985**, 1305. (b) Yaghi, O. M.; Davis, C. E.; Li, G.; Li, H. *J. Am. Chem. Soc.* **1997**, *119*, 2861. (c) Li, H.; Davis, C. E.; Groy, T. L.; Kelley, D. G.; Yaghi, O. M. *J. Am. Chem. Soc.* **1998**, *120*, 2186.

(4) Shores, M. P.; Beauvais, L. G.; Long, J. R. *J. Am. Chem. Soc.* **1999**, *121*, 775.

(5) Shores, M. P.; Beauvais, L. G.; Long, J. R. *Inorg. Chem.* **1999**, *38*, 1648.

(6) Selected references: (a) Manriquez, J. M.; Yee, G. T.; McLean, R. S.; Epstein, A. J.; Miller, J. S. *Science* **1991**, *252*, 1415. (b) Real, J. A.; Munno, G. D.; Muñoz, M. C.; Julve, M. *Inorg. Chem.* **1991**, *30*, 2701. (c) Mallah, T.; Thiébaut, S.; Verdaguer, M.; Veillet, P. *Science* **1993**, *262*, 1554. (d) Entley, W. R.; Girolami, G. S. *Science* **1995**, *268*, 397. (e) Sato, O.; Iyoda, T.; Fujishama, A.; Hashimoto, K. *Science* **1996**, *271*, 49. (f) Sato, O.; Iyoda, T.; Fujishama, A.; Hashimoto, K. *Science* **1996**, *272*, 704. (g) Mathonière, C.; Nuttall, C. J.; Carling, S. G.; Day, P. *Inorg. Chem.* **1996**, *35*, 1201. (h) Kahn, O.; Martinez, C. J. *Science* **1998**, *279*, 44. (i) Larionova, J.; Clérac, R.; Sanchiz, J.; Kahn, O.; Golhen, S.; Ouahab, L. *J. Am. Chem. Soc.* **1998**, *120*, 13088. (j) Ohkoshi, S.; Abe, Y.; Fujishima, A.; Hashimoto, K. *Phys. Rev. Lett.* **1999**, *82*, 1285.

10.1021/ja994186h CCC: $19.00
Published on Web 03/04/2000

approach is apparent from further demonstrations of its use in constructing electrical conductors[7] and nonlinear optical materials.[8] An appealing, yet less-explored, potential application lies in the development of chemical sensors.

Due to stricter chemical exposure guidelines for the workplace and growing concern over chemical releases into the environment, the efficient and reliable detection of volatile organic compounds has become important. As a result, much recent research has focused on developing chemical sensors with the ability to detect and identify solvent vapors. Ideally, robust materials displaying rapid and significant changes in their optical absorption or emission spectra upon exposure to solvent vapors (vapochromism) are sought for such applications. To this end, molecular compounds with weak intermolecular interactions that are readily perturbed by an absorbed solvent have been studied extensively. Particularly striking examples are compounds of the type $[Pt(NCAr)_4][M(CN)_4]$ (M = Pd, Pt), which display shifts in their absorption and emission maxima upon exposure to vapors of solvents such as water, acetonitrile, ether, acetone, benzene, hexanes, chlorinated alkanes, and alcohols.[9] Similarly, solid $Au_3(CH_3N{=}COCH_3)_3$ luminesces upon exposure to chloroform, dichloromethane, toluene, methanol, hexane, or water,[10] while $[Au(S_2CN(C_5H_{11})_2)]_2$ displays this effect only upon exposure to aprotic polar solvents.[11] Other approaches have focused on incorporating established solvatochromic molecules or ions into solid materials. For example, the $[(Ph_3P)_2N]^+$ salt of the solvatochromic $[Ru(bpy)(CN)_4]^{2-}$ complex can function as a humidity sensor.[12] Encapsulation of the dye Nile Red in zeolite Y[13] or incorporation of luminescent Tb^{3+} ions into the framework of a microporous solid[14] permit shape and size selective sensing. Indeed, this type of selectivity is a distinct advantage of extended framework sensing materials.

Resembling enlarged cyanometalate ions, the recently prepared $[Re_6Q_8(CN)_6]^{4-}$ (Q = S, Se, Te) clusters[15,16] exhibit a geometry consisting of an Re_6 octahedron with each face capped by a μ_3-Q atom and a terminal cyanide ligand extending from each Re apex. The greater size of the cluster ions, however, suggests that their substitution into known cyanometalate-based solids could enlarge extant framework cavities, leading to materials with enhanced inclusion properties. Thus far, the metal−cyanide frameworks of Prussian blue ($Fe_4[Fe(CN)_6]_3\cdot 14H_2O$),[17] $Na_2Zn_3[Fe(CN)_6]_2\cdot 9H_2O$,[18] and $[Mn_2(H_2O)_4][Ru(CN)_6]\cdot 4H_2O$[19] have all been successfully expanded using just this strategy.[4,5,20] In addition, a range of new layered and porous structures containing Mn^{2+}, Fe^{2+}, Co^{2+}, Ni^{2+}, Zn^{2+}, and Cd^{2+} ions spaced apart by the Re_6 clusters has been generated.[15,20,21] Frequently, the metal ions incorporated in these open framework structures exhibit one or more coordinated water molecules that can be removed by thermolysis to produce accessible, vacant metal coordination sites.

Herein, we demonstrate how Co^{2+} ions, well-known for the dramatic color changes associated with their facile interconversion between octahedral and tetrahedral coordination geometries, can be incorporated into porous solids to produce materials capable of detecting and identifying volatile organic compounds.

Experimental Section

Preparation of Compounds. The compounds $Na_4[Re_6Q_8(CN)_6]$ (Q = S, Se), $NaCs_3[Re_6Q_8(CN)_6]$ (Q = S, Se), and $Cs_2[Co(H_2O)_2]_3[Re_6Se_8(CN)_6]_2\cdot 12H_2O$ were prepared as described previously.[4,5,15,16] Water was distilled and deionized with a Milli-Q filtering system. Other reagents were of commercial origin, and were used as received. The water content of each compound was determined by thermogravimetric analysis. Product identity and purity were verified by comparison of the observed X-ray powder diffraction pattern with a calculated pattern generated from the single-crystal results.

$[Co_2(H_2O)_4][Re_6S_8(CN)_6]\cdot 10H_2O$ (1). A 50 mL aqueous solution of $Co(NO_3)_2\cdot 6H_2O$ (0.32 g, 1.1 mmol) was added to a 250 mL aqueous solution of $NaCs_3[Re_6S_8(CN)_6]$ (0.31 g, 0.16 mmol). The volume of the solution was reduced to 75 mL by heating at 60 °C, resulting in an orange precipitate. The solid was collected by centrifugation, washed with successive aliquots of water (3 × 25 mL), and dried in air to give 0.24 g (81%) of orange crystalline product. IR (KBr): ν_{CN} 2156 cm^{-1}. μ_{eff} = 6.97 μ_B at 295 K. Anal. Calcd for $C_6H_{28}Co_2N_6O_{14}Re_6S_8$: C, 3.79; H, 1.49; Co, 6.20; N, 4.42; Na, 0.00; Re, 58.8. Found: C, 3.77; H, 1.46; Co, 6.34; N, 4.37; Na, <0.03; Re, 58 ± 2.

$Cs_2[Co(H_2O)_2][Re_6S_8(CN)_6]\cdot 2H_2O$ (2). An 8 mL aqueous solution of $Co(NO_3)_2\cdot 6H_2O$ (0.050 g, 0.17 mmol) was combined with a 10 mL aqueous solution of $NaCs_3[Re_6S_8(CN)_6]$ (0.15 g, 0.077 mmol) and stirred for 12 h to give an orange precipitate. The solid was collected by centrifugation, washed with successive aliquots of water (3 × 25 mL), and dried in air to give 0.10 g (69%) of product. IR (KBr): ν_{CN} 2137 cm^{-1}. Anal. Calcd for $C_6H_8CoCs_2N_6O_4Re_6S_8$: C, 3.74; H, 0.42; N, 4.36. Found: C, 4.19; H, 0.49; N, 4.70.

$[Co(H_2O)_3]_4[Co_2(H_2O)_4][Re_6Se_8(CN)_6]_3\cdot 44H_2O$ (3). A 10 mL aqueous solution of $Co(NO_3)_2\cdot 6H_2O$ (0.15 g, 0.52 mmol) was combined with a 10 mL aqueous solution of $Na_4[Re_6Se_8(CN)_6]$ (0.21 g, 0.11 mmol) and stirred for 30 min to give an orange microcrystalline precipitate. The solid was collected by centrifugation, washed with successive aliquots of water (3 × 25 mL), and dried in air to give 0.17 g (65%) of product. IR (KBr): ν_{CN} 2032 cm^{-1}. μ_{eff} = 12.5 μ_B at 295 K. Anal. Calcd for $C_{18}H_{120}Co_6N_{18}O_{60}Re_{18}Se_{24}$: C, 3.02; H, 1.69; Co, 4.95; N, 3.53; Na, 0.00; Re, 46.9. Found: C, 3.20; H, 1.54; Co, 4.72; N, 3.45, Na, <0.03; Re, 46.8 ± 0.7.

X-ray Structure Determinations. Single crystals of compounds **1** (orange rectangular plates) and **3** (orange rods) were grown by layering aqueous solutions of the reactants in a narrow diameter tube. The crystals were coated in Paratone-N oil, attached to quartz fibers, transferred to a Bruker SMART diffractometer, and cooled in a dinitrogen stream. Lattice parameters were initially determined from a least squares refinement of more than 53 carefully centered reflections. The raw intensity data were converted (including corrections for background and Lorentz and polarization effects) to structure factor amplitudes and their esd's using the SAINT 4.15 program. An empirical absorption correction was applied to each data set using SADABS.

(7) (a) Aumüller, A.; Erk, P.; Klebe, G.; Hünig, S.; von Schütz, J. U.; Werner, H.-P. *Angew. Chem., Int. Ed. Engl.* **1986**, *25*, 740. (b) Ermer, O. *Adv. Mater.* **1991**, *3*, 608.

(8) (a) Bénard, S.; Yu, P.; Coradin, T.; Rivière, E.; Nakatani, K.; Clément, R. *Adv. Mater.* **1997**, *9*, 981. (b) Huang, S. D.; Xiong, R.-G. *Polyhedron* **1997**, *16*, 3929. (c) Lin, W.; Evans, O. R.; Xiong, R.-G.; Wang, Z. *J. Am. Chem. Soc.* **1998**, *120*, 13272.

(9) (a) Exstrom, C. L.; Sowa, J. R.; Daws, C. A.; Janzen, D. E.; Mann, K. R. *Chem. Mater.* **1995**, *7*, 15. (b) Daws, C. A.; Exstrom, C. L.; Sowa, J. R.; Mann, K. R. *Chem. Mater.* **1997**, *9*, 363. (c) Buss, C. E.; Anderson, C. E.; Pomije, M. K.; Lutz, C. L.; Britton, D.; Mann, K. R. *J. Am. Chem. Soc.* **1998**, *120*, 7783. (d) Exstrom, C. L.; Pomije, M. K.; Mann, K. R. *Chem. Mater.* **1998**, *10*, 942.

(10) Vickery, J. C.; Olmstead, M. M.; Fung, E. Y.; Balch, A. L. *Angew. Chem., Int. Ed. Engl.* **1997**, *36*, 1179.

(11) Mansour, M. A.; Connick, W. B.; Lachicotte, R. J.; Gysling, H. J.; Eisenberg, R. *J. Am. Chem. Soc.* **1998**, *120*, 1329.

(12) Evju, J. K.; Mann, K. R. *Chem. Mater.* **1999**, *11*, 1425.

(13) Meinershagen, J. L.; Bein, T. *J. Am. Chem. Soc.* **1999**, *121*, 448.

(14) Reineke, T. M.; Eddaoudi, M.; Fehr, M.; Kelley, D.; Yaghi, O. M. *J. Am. Chem. Soc.* **1999**, *121*, 1651.

(15) Beauvais, L. G.; Shores, M. P.; Long, J. R. *Chem. Mater.* **1998**, *10*, 3783.

(16) Mironov, Y. V.; Cody, J. A.; Albrecht-Schmitt, T. E.; Ibers, J. A. *J. Am. Chem. Soc.* **1997**, *119*, 493.

(17) Buser, H. J.; Schwarzenbach, D.; Petter, W.; Ludi, A. *Inorg. Chem.* **1977**, *16*, 2704.

(18) Garnier, E.; Gravereau, P.; Hardy, A. *Acta Crystallogr.* **1982**, *B38*, 1401.

(19) Rüegg, M.; Ludi, A.; Rieder, K. *Inorg. Chem.* **1971**, *10*, 1773.

(20) Bennett, M. V.; Shores, M. P.; Beauvais, L. G.; Long, J. R. Submitted for publication.

(21) Naumov, N. G.; Virovets, A. V.; Sokolov, M. N.; Artemkina, S. B.; Fedorov, V. E. *Angew. Chem., Int. Ed. Engl.* **1998**, *37*, 1943.

Table 1. Crystallographic Data and Structure Refinement Parameters for $[Co_2(H_2O)_4][Re_6S_8(CN)_6]\cdot 12H_2O$ (**1**·$2H_2O$), $Cs_2[Co(H_2O)_2][Re_6S_8(CN)_6]\cdot 2H_2O$ (**2**), and $[Co_2(H_2O)_4][Co(H_2O)_3]_4[Re_6Se_8(CN)_6]_3\cdot 44H_2O$ (**3**)

	1·$2H_2O$[a]	**2**[b]	**3**[a]
formula	$C_6H_{32}Co_2N_6O_{16}Re_6S_8$	$C_6H_4CoCs_2N_6O_2Re_6S_8$	$C_{18}H_{120}Co_6N_{18}O_{60}Re_{18}Se_{24}$
formula wt	1935.92	1890.59	7149.54
T, K	173	295	158
space group	$P2_1/n$	*Imma*	*C2/c*
Z	2	4	4
a, Å	9.7438(3)	18.4651(6)	26.546(1)
b, Å	16.3262(6)	10.6368(3)	27.3516(9)
c, Å	12.3331(4)	13.3162(4)	18.2899(8)
β, deg	97.117(1)		91.178(2)
V, Å^3	1946.8(1)	2615.4(1)	13277.0(9)
d_{calc}, g/cm^3	3.302	4.801	3.577
R_1, wR_2,[c] %	2.67, 5.13		7.31, 12.37
R_p, wR_p, R_{F2},[d] %		10.83, 13.87, 7.66	

[a] Obtained using graphite monochromated Mo Kα ($\lambda = 0.71073$ Å) radiation. [b] Obtained using synchrotron radiation of wavelength $\lambda = 1.5432$ Å. [c] $R_1 = \sum||F_o| - |F_c||/\sum|F_o|$; $wR_2 = \{\sum[w(|F_o| - |F_c|)^2]/\sum[w(|F_o|^2)]\}^{1/2}$. [d] $R_p = \sum|y_i(\text{obs}) - y_i(\text{calc})|/\sum y_i(\text{obs})$; $wR_p = \{\sum[w_i(y_i(\text{obs}) - y_i(\text{calc}))^2/\sum[w_i(y_i(\text{obs}))^2]\}^{1/2}$; $R_{F2} = \sum|F_o^2 - F_c^2|/\sum F_o^2$.

Space group assignments were based on systematic absences, E statistics, and successful refinement of the structures. Structures were solved by direct methods, with the aid of difference Fourier maps, and were refined with successive full-matrix least-squares cycles. Two of the six lattice water molecules in the structure of **1**·$2H_2O$ are disordered over multiple positions, and were modeled with partial occupancies. Partially occupied atoms in this structure were refined isotropically, while all other atoms were refined anisotropically. Lattice water molecules in the structure of **3** were refined with anti-bumping restraints; 15 of the 35 waters are disordered over multiple positions and were modeled accordingly. Owing to the disorder, the water content of the crystal could not be reliably determined from the structural refinement. Light atoms ($Z < 9$) in this structure were refined isotropically, while all the other atoms were refined anisotropically. Hydrogen atoms were not included in either of the refinements. Crystallographic parameters are listed in Table 1.

High-resolution X-ray powder diffraction data were collected at beamline 2-1 of the Stanford Synchrotron Radiation Laboratory using a finely ground sample of compound **2** loaded onto a zero-background silicon plate. X-rays of wavelength 1.5432 Å were selected using a Si(111) monochromator. The pattern was scanned in the 8−55° and 48−110° 2θ range with 0.008° and 0.02° steps, respectively, using 2° rocking scans. The wavelength, zero point, and profile parameters were refined using NIST standard SRM660 (LaB_6). The previously determined crystal structure of $Cs_2[Fe(H_2O)_2][Re_6S_8(CN)_6]$[15] was used as the starting model for a simultaneous Rietveld refinement against both the low and high angle data using the program GSAS.[22] A cosine Fourier series background and a pseudo-Voigt peak shape,[23] corrected for asymmetry[24] and anisotropic peak broadening arising from the plate morphology,[25] were also refined. The peak asymmetry and anisotropy were too highly correlated to be refined successfully; hence, only the high angle data were used in subsequent refinement cycles. The well-established molecular geometry of the $[Re_6S_8(CN)_6]^{4-}$ cluster[15] was maintained by applying the following constraints: Re−Re 2.6(1) Å, Re−S 2.41(2) Å, Re−C 2.15(3) Å, C−N 1.14(2) Å, and Co−N 2.1(1) Å. Isotropic thermal parameters were refined for the Cs, Co, Re, and S atoms. Thermal parameters for the lighter atoms were not refined: isotropic temperature factors were fixed at 0.03 Å^2 for C and N atoms and 0.06 Å^2 for O atoms of the bound water molecules. Difficulties in refining the anisotropic peak broadening arose due to the overlap of peaks and resulted in somewhat high R values. Crystallographic parameters are listed in Table 1.

Diffuse Reflectance UV−vis Spectroscopy. The method used was based on a previously reported technique.[9b] Solid samples were ground with a mortar and pestle and spread onto 0.8 × 3.0 cm strips of filter paper (Whatman No. 1). Each coated strip was held against the inner surface of a quartz cuvette with a spring, and a piece of glass wool was placed in the cuvette to serve as the solvent reservoir. The glass wool was doused with solvent, and the cell was covered and allowed to stand for at least 10 min before measuring the reflectance spectrum of the sample. Spectra were acquired relative to $BaSO_4$ on a Perkin-Elmer Lambda 9 spectrophotometer equipped with a 60 mm integrating sphere.

Other Physical Measurements. Routine X-ray powder diffraction data were collected using Cu Kα ($\lambda = 1.5406$ Å) radiation on a Siemens D5000 diffractometer or, for samples sealed in capillaries, on an instrument equipped with an INEL curved position sensitive detector. Magnetic susceptibility measurements were carried out on a Quantum Design SQUID magnetometer. Thermogravimetric analyses were performed in a dinitrogen atmosphere at a ramp rate of 1 deg C/min, using a TA Instruments TGA 2950. Infrared spectra were recorded on a Mattson Infinity System FTIR spectrometer or on a Bruker IFS 66v/s FTIR spectrometer equipped with a horizontal attenuated total reflectance accessory.

Results and Discussion

Syntheses. Compounds **1**, **2**, and **3** form upon addition of an aqueous solution containing cobaltous ions to an aqueous solution of $Na_4[Re_6Q_8(CN)_6]$ (Q = S, Se) or $NaCs_3[Re_6Q_8(CN)_6]$, in accord with the following general reaction.

$$xA^+ + \left(2 - \frac{x}{2}\right)[Co_2(H_2O)_6]^{2+} + [Re_6Q_8(CN)_6]^{4-} \rightarrow A_xCo_{2-(x/2)}[Re_6Q_8(CN)_6]\cdot yH_2O \quad (1)$$

Although the choices of chalcogen (Q) and alkali metal cation (A^+) influence the structure formed, the ratio of Co^{2+} ions to Re_6 clusters only affects the product when $NaCs_3[Re_6S_8(CN)_6]$ is employed as the cluster source. In this case, a 5:1 molar ratio yields $[Co_2(H_2O)_4][Re_6S_8(CN)_6]\cdot 10H_2O$ (**1**), while a 2:1 molar ratio results in the immediate precipitation of $Cs_2[Co(H_2O)_2][Re_6S_8(CN)_6]\cdot 2H_2O$ (**2**). The corresponding Q = Se cluster source affords the previously reported compound $Cs_2[Co(H_2O)_2]_3[Re_6Se_8(CN)_6]_2\cdot 12H_2O$,[15] regardless of the stoichiometry of the reactants. Presumably, the affinity of the Cs^+ ions for the soft cyanide ligands leads to their inclusion in these phases. In contrast, reactions utilizing $Na_4[Re_6Q_8(CN)_6]$ produce only the neutral frameworks of compounds **1** and $[Co(H_2O)_3]_4[Co_2(H_2O)_4][Re_6Se_8(CN)_6]_3\cdot 44H_2O$ (**3**) for the S- and Se-containing clusters, respectively. Similar reactions between Co^{2+} ions and $[Re_6Te_8(CN)_6]^{4-}$ resulted in amorphous products.

Structures. The crystal structure of $[Co_2(H_2O)_4][Re_6S_8(CN)_6]\cdot 12H_2O$ (**1**·$2H_2O$)[26] reveals a three-dimensional framework composed of $[Re_6S_8]^{2+}$ and $[Co_2(\mu\text{-}OH_2)_2]^{4+}$ cluster cores linked through cyanide bridges. Mean interatomic distances and angles are listed in Table 2, along with those of the other reported structures. The octahedral coordination environment of each Co^{2+} ion consists of three nitrogen atoms from cyanide ligands and three water ligands bound in a *fac* configuration. Two of these water ligands bridge to another Co^{2+} ion, creating a rhombic $[Co_2(\mu\text{-}OH_2)_2]^{4+}$ unit that is surrounded by six rhenium clusters in a distorted octahedral arrangement (Figure 1). In turn, each Re_6 moiety is connected to six Co_2 units to give a Prussian blue type structure with rhenium and cobalt

(22) Larson, A. C.; von Dreele, R. B. *GSAS: General Structure Analysis System*; Los Alamos National Laboratory: Los Alamos, NM, 1990.

(23) Thompson, P.; Cox, D. E.; Hastings, J. B. *J. Appl. Crystallogr.* **1987**, *20*, 79.

(24) Finger, L. W.; Cox, D. E.; Jephcoat, A. P. *J. Appl. Crystallogr.* **1994**, *27*, 892.

(25) Stephens, P. W. *J. Appl. Crystallogr.* **1999**, *32*, 281.

(26) Note that the water content of the crystal pulled directly from the mother liquor is slightly higher than that of the air-dried product.

Table 2. Selected Mean Interatomic Distances (Å) and Angles (deg) from the Structures of $[Co_2(H_2O)_4][Re_6S_8(CN)_6]\cdot 12H_2O$ (**1**·2H$_2$O), $Cs_2[Co(H_2O)_2][Re_6S_8(CN)_6]\cdot 2H_2O$ (**2**), and $[Co_2(H_2O)_4][Co(H_2O)_3]_4[Re_6Se_8(CN)_6]_3\cdot 44H_2O$ (**3**)[a]

	1·2H$_2$O	**2**	**3**
Re−Re	2.606(3)	2.615(9)	2.635(6)
Re−Q	2.415(6)	2.40(3)	2.527(8)
Re−C	2.111(1)	2.14(1)	2.09(4)
C−N	1.150(6)	1.14(1)	1.17(5)
Co−N	2.067(8)	2.18(2)	2.08(3)
Co−O(t)	2.118	2.24(5)	2.15(2)
Co−O(μ)	2.18(2)		2.23(1)
Co···Co	3.379		3.390
Re−C−N	176.1(4)	172(2)	175(3)
Co−N−C	173(2)	168.8	163(8)
O(μ)−Co−O(μ)	79		81
Co−O(μ)−Co	101.1		98.9

[a] t = terminal, μ = bridging.

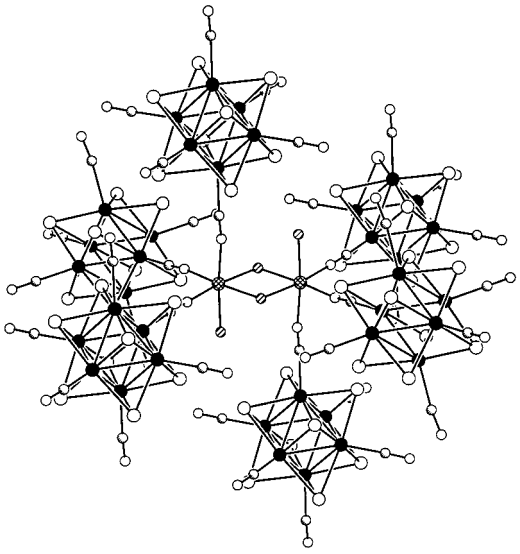

Figure 1. Local environment of the $[Co_2(H_2O)_4]^{4+}$ clusters in the structure of **1**·2H$_2$O. Large black, white, and crosshatched spheres represent Re, S, and Co atoms, respectively, while smaller highlighted, white, and diagonally shaded spheres represent C, N, and O atoms, respectively. The Co_2 and Re_6 clusters reside on crystallographic inversion centers.

clusters occupying alternating metal ion sites. The sizable clusters result in an overall expansion of the framework, including its cavities, which are defined by the large cubelike cage unit depicted in Figure 2. Each cage demarcates a volume of 258 Å^3 (based on estimated van der Waals radii of the framework atoms),[27] such that, overall, the framework comprises only 47% of the total volume of the structure. An individual cavity is filled with a hydrogen-bonded aggregate of six solvate water molecules. Access to its interior is through the faces of the cage, which exhibit dimensions of approximately 3.7 × 3.8 and 4.6 × 6.2 Å for the smallest and largest openings, respectively, and 4.2 × 4.8 Å for the other four equivalent openings. The alternating orientations of neighboring cages permit an incoming guest molecule to penetrate the framework without ever passing through the smallest openings. The planes of the Co_2O_2 rhombs in the structure are oriented perpendicular to the large and small cage faces, making compound **1** a direct expansion of the metal−cyanide framework of $[Mn_2(H_2O)_4][Ru(CN)_6]\cdot 4H_2O$,[19] with Co^{2+} ions and $[Re_6S_8]^{2+}$ cluster cores replacing the Mn^{2+} and Ru^{2+} ions, respectively. The recently

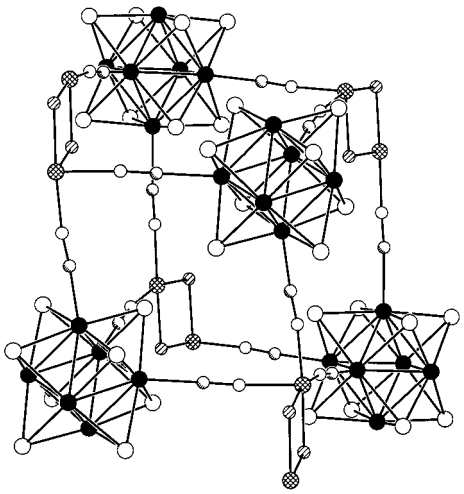

Figure 2. Cubelike cage unit defining the cavities in the structure of **1**·2H$_2$O. Atom types are as designated in Figure 1. The small and large openings into the cavities correspond to the front and rear cage faces, respectively.

prepared cluster-cyanide compound $[Cd_2(H_2O)_4]_2[Re_6S_8(CN)_6]\cdot 14H_2O$ exhibits a remarkably similar framework, differing primarily in that the planes of the Cd_2O_2 rhombs are oriented *parallel* to the large and small faces of its cubelike cages.[5]

The structure of $Cs_2[Co(H_2O)_2][Re_6S_8(CN)_6]\cdot 2H_2O$ (**2**) was established with a Rietveld refinement against synchrotron X-ray powder diffraction data (see Supporting Information), using the atomic coordinates of the isotypic compound $Cs_2[Fe(H_2O)_2][Re_6S_8(CN)_6]$[15] as an initial model. Its framework comprises two-dimensional anionic sheets consisting of a square lattice of alternating $[Re_6S_8]^{2+}$ cluster cores and Co^{2+} ions linked by cyanide bridges. Each Co^{2+} ion is bound by the nitrogen terminus of four cyanide ligands, with two trans water molecules completing its octahedral coordination sphere, as depicted in Figure 3. Likewise, each rhenium cluster is connected through only four cyanide ligands, leaving two trans cyanide ligands uncoordinated. The structure is reminiscent of the Hoffman clathrate phases, with $[Re_6S_8(CN)_6]^{4-}$ and $[Co(H_2O)_2]^{2+}$ replacing the $[Ni(CN)_4]^{2-}$ and $[Ni(NH_3)_2]^{2+}$ components, respectively.[28] However, in contrast to the rigorously planar network of $[Ni(NH_3)_2][Ni(CN)_4]\cdot 2C_6H_6$, the charged sheets in compound **2** are ruffled along square diagonals (the *a* axis) due to interactions between the terminal cyanide ligands and Cs^+ ions sandwiched between the layers. These electrostatic interactions appear to prohibit any analogous clathrate behavior.

The structure of $[Co(H_2O)_3]_4[Co_2(H_2O)_4][Re_6Se_8(CN)_6]_3\cdot 44H_2O$ (**3**) consists of a mixture of Co^{2+} ions and $[Co_2(\mu\text{-}OH_2)_2]^{4+}$ units connected through $[Re_6Se_8(CN)_6]^{4-}$ clusters. The isolated Co^{2+} centers display an octahedral coordination geometry, with three N-bound cyanide ligands and three water molecules arranged in a *mer* configuration. The Co_2 clusters are essentially identical with those found in the structure of **1**·2H$_2$O (see Figure 1, above) except that the Co−N−C angles are slightly more bent, as apparent from the mean values listed in Table 2. Each rhenium cluster is connected to four isolated Co^{2+} ions and two Co_2 clusters. Three of these clusters are joined via Re−CN−Co−NC−Re linkages to form a triangular moiety. Two triangular units are then fused through Re−CN−Co bridges to create a trigonal antiprismatic $[Co_2(H_2O)_4]_2[Co(H_2O)_3]_4[Re_6Se_8(CN)_6]_6$ cage. The isolated Co^{2+} ions bridge strictly within the cages, while the Co_2 units interconnect cages

(27) The void volume was determined using a Monte Carlo integration procedure described previously.[15]

(28) (a) Rayner, J. H.; Powell, H. M. *J. Chem. Soc.* **1952**, 319. (b) Rayner, J. H.; Powell, H. M. *J. Chem. Soc.* **1958**, 3412.

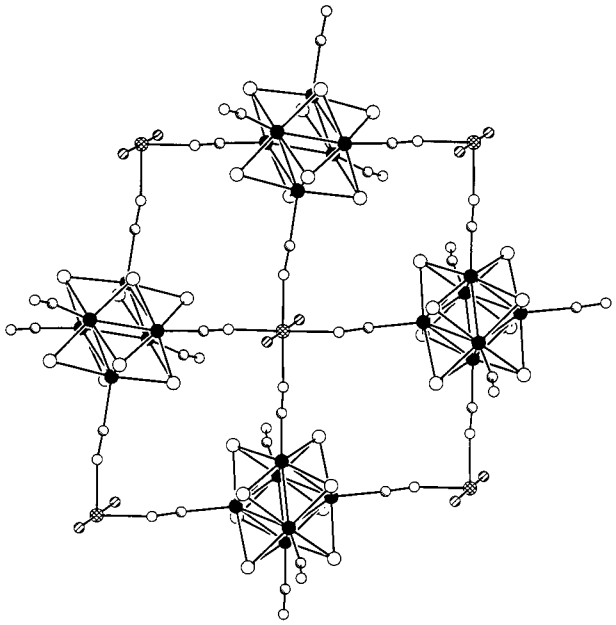

Figure 3. Local coordination environment of a Co^{2+} ion in the structure of **2**. Atom types are again as designated in Figure 1. Note that the Re−C−N−Co linkages are not perfectly linear, leading to a ruffling of the sheets that comprise the structure. Crystallographic mirror planes containing the Co and O atoms run diagonally, intersecting at the central Co atom. Twofold rotation axes lie along these intersections, penetrating each Co atom.

to form a one-dimensional channel (Figure 4) with a minimum diameter of 4.8 Å, based on estimated van der Waals radii of the framework atoms. Each Re_6 cluster is shared between two adjacent cages to create a hexagonal array of the channels. The framework atoms occupy only 56% of the volume in this structure.[27] As prepared, water ligands on isolated Co^{2+} ions protrude into the channels and participate in forming a complex hydrogen-bonded network with the lattice water molecules.

The assignment of the Co_2 cluster cores in the structures of **1**·2H_2O and **3** as $[Co^{II}_2(\mu\text{-}OH_2)_2]^{4+}$ instead of $[Co^{III}_2(\mu\text{-}OH)_2]^{4+}$ is consistent with the attributes of previously established compounds. The mean Co−O distances within the Co_2O_2 rhombs are 2.18(2) and 2.23(1) Å for the two structures, respectively. These distances are in rough agreement with those observed in molecular clusters featuring $[Co_2(\mu\text{-}OH_2)(\mu\text{-}O_2CR)_2]^{2+}$ cores, which range from 2.111(5) to 2.18(1) Å.[29] Considerably shorter distances would be expected for hydroxo-bridged Co^{III}_2 or Co^{II}_2 units: witness the mean Co−O separations of 1.925(2) and 2.01(3) Å in $[Co_2(OH)_2(en)_4](NO_3)_4$[30] and $[Co_2(OH)_2((3,5\text{-}^i\text{Pr-1-pyrazolyl})_3HB)_2]$,[31] respectively. In addition, no O−H stretching absorption peaks characteristic of bridging hydroxide were apparent in the infrared spectra of compounds **1** and **3**. Finally, the magnetic susceptibilities of the compounds indicate the presence of paramagnetic Co^{II} rather than diamagnetic Co^{III} centers. At 295 K, μ_{eff} values for **1** and **3** were measured to be 6.97 μ_B (4.93 μ_B per Co) and 12.5 μ_B (5.10 μ_B per Co), respectively, well within the expected range of 4.77 to 5.40 μ_B per octahedral Co^{II} center.[32]

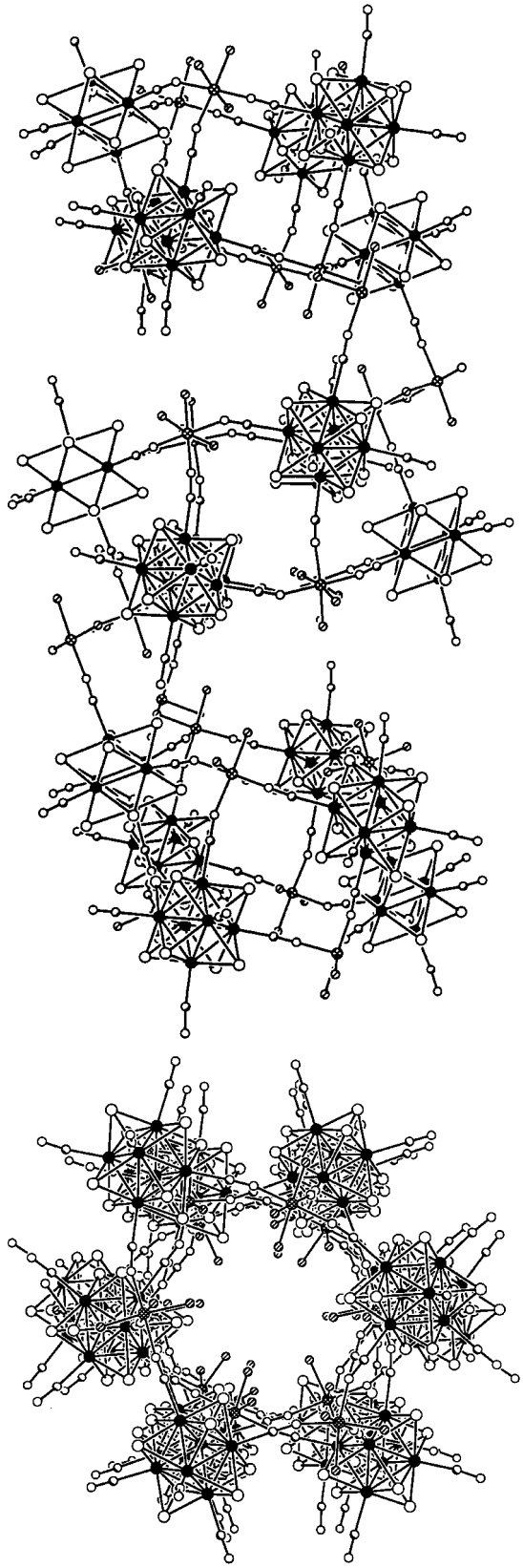

Figure 4. A one-dimensional channel from the structure of **3**; solvate water molecules are not shown for clarity. Large black, white, and crosshatched spheres represent Re, Se, and Co atoms, respectively, while smaller highlighted, white, and diagonally shaded spheres represent C, N, and O atoms, respectively. Upper: A side-on view of the portion of the framework that defines the channel, showing the connectivity of the trigonal antiprismatic cages. Lower: A perpendicular view looking directly down the channel. Notice how the bound water ligands protrude into the channel.

(29) (a) Hänggi, G.; Schmalle, H.; Dubler, E. *Acta Crystallogr.* **1992**, *C48*, 1008. (b) Coucouvanis, D.; Reynolds, R. A.; Dunham, W. R. *J. Am. Chem. Soc.* **1995**, *117*, 7570. (c) Corkery, R. W.; Hockless, D. C. R. *Acta Crystallogr.* **1997**, *C53*, 840.

(30) Thewalt, U.; Zehnder, M. *Helv. Chim. Acta* **1977**, *60*, 2000.

(31) Kitajima, N.; Hikichi, S.; Tanaka, M.; Moro-oka, Y. *J. Am. Chem. Soc.* **1993**, *115*, 5496.

(32) Banci, L.; Bencini, A.; Benelli, C.; Gatteschi, D.; Zanchini, C. *Struct. Bonding* **1982**, *52*, 37.

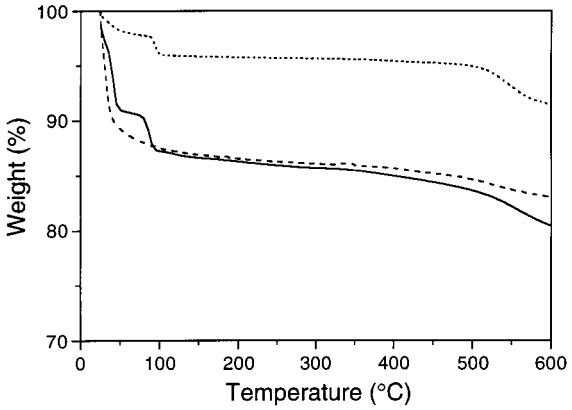

Figure 5. Thermogravimetric analysis showing the weight loss in compounds **1** (solid line), **2** (dashed line), and **3** (dotted line). Note that compounds **1** and **2** release water in two steps, corresponding to the initial loss of lattice water molecules, followed by release of the bound water ligands. All three compounds are compositionally stable up to ca. 500 °C.

Such unsupported water bridges between transition metal centers are not without precedent. Single water bridges of the type M−(μ-H_2O)−M have been identified in the molecular species $[Ag_4(H_2O)_2(NO_3)_2]^{2+}$;[33] however, they are predominately encountered linking transition metal centers into one-dimensional chains.[34−38] For example, the compounds $[CoL_2(H_2O)_3]$ (L = *N*-benzoylglycinate,[34] 3,6-dichloro-2-methoxybenzoate,[35] 2,6-dimethoxybenzoate,[36] and 3-hydroxy-4-methoxybenzoate[37]) exhibit chains of Co^{2+} ions connected solely via single water molecules, with Co−O bond lengths ranging from 2.069(5) to 2.270(1) Å. More pertinently, M−(μ-H_2O)$_2$−M units with two water molecules bridging divalent transition metal centers have been observed in one-dimensional chains,[39] two-dimensional sheets,[40,41] and three-dimensional frameworks.[5,19] Particularly relevant examples include the aforementioned solids $[Mn_2(H_2O)_4][Ru(CN)_6]\cdot 4H_2O$[19] and $[Cd_2(H_2O)_4]_2[Re_6S_8(CN)_6]\cdot 14H_2O$[5] which are structurally analogous to compound **1**, as well as the compound $[Cd_2(H_2O)_4][Cu(CN)_3]_2\cdot 4H_2O$,[40] wherein $[Cd_2(H_2O)_4]^{4+}$ clusters are connected through triangular $[Cu(CN)_3]^{2-}$ units to form two-dimensional sheets. An important feature common to *all* of these structures is the stabilization of the weakly bound bridging water ligands via hydrogen-bonding interactions, typically with solvate water molecules. Indeed, hydrogen-bonded water networks (with O···O distances between 2.62 and 3.00 Å, within the range usually associated with hydrogen bonding)[42] extending through the cages and channels in the structures of **1**·2H_2O and **3** are anchored to terminal and bridging water ligands on the Co^{2+} ions. The bridging water ligands utilize both of their hydrogen atoms in forming hydrogen bonds to two solvate water molecules located at O···O separations of 2.67 and 2.70 Å in **1**·2H_2O and 2.62 and 2.81 Å in **3**. In addition, each of these solvate water molecules is within hydrogen-bonding distance of a terminal water ligand, potentially providing further stabilization of the $[Co_2(H_2O)_4]^{4+}$ cluster. The situation is illustrated below with a portion of the crystal structure of compound **3**.

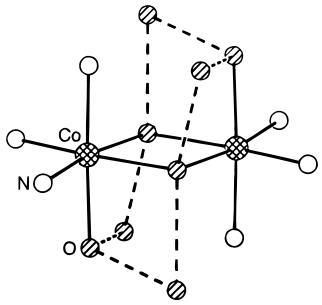

Thermal Stability. The thermal stability of each new compound was probed by thermogravimetric analysis (see Figure 5). The results for compound **1** indicate that ten of its water molecules are released by 50 °C, followed by loss of the remaining four water molecules by 100 °C; presumably the two steps correspond to the loss of solvate and bound water molecules, respectively. Compound **2** exhibits a similar behavior, which can be attributed to release of the two solvate water molecules by 86 °C, and subsequent loss of the two bound water ligands by 100 °C. In contrast, the data for compound **3** reveal a continuous loss of water up to its complete dehydration at ca. 100 °C. The compounds then display only minor (<2%) mass loss up to approximately 500 °C. The rather more substantial losses occurring in this temperature regime for Prussian blue[43] and $K_2Zn_3[Fe(CN)_6]_2\cdot 8.5H_2O$[44] have been attributed to the evolution of cyanogen from the surface of the crystallites. Thus, the frameworks of compounds **1**−**3** are compositionally more robust than those of most noncluster metal−cyanide materials. However, X-ray powder diffraction patterns collected on samples heated at constant temperature for 16 h indicate that compounds **1** and **3** undergo irreversible transitions to new and as yet unidentified structures upon dehydration at approximately 100 °C. This is perhaps to be expected, given the pivotal roles of the bridging water molecules in their frameworks. Compound **2** retains its crystallinity unless heated above ca. 300 °C.

Vapochromic Behavior. As shown in Figure 6, orange solid samples of $[Co_2(H_2O)_4][Re_6S_8(CN)_6]\cdot 10H_2O$ (**1**) and $[Co(H_2O)_3]_4[Co_2(H_2O)_4][Re_6Se_8(CN)_6]_3\cdot 44H_2O$ (**3**) display striking color changes upon exposure to certain solvents in either the vapor or liquid phase. For example, exposure to diethyl ether vapor immediately turns the solids an intense blue-violet or blue color. Other solvents produce a range of different colors, including the red-violet and green colors observed for compounds **1** and **3**, respectively, in the presence of tetrahydrofuran. These changes are all reversible, with the original orange color being quickly regained in an ambient solvent-free atmosphere.[45] In contrast, no deviation from the original orange color of Cs_2-

(33) Schöllhorn, H.; Thewalt, U.; Lippert, B. *Inorg. Chim. Acta* **1987**, *135*, 155.
(34) (a) Eichelberger, H.; Majeste, R.; Surgi, R.; Trefonas, L.; Good, M. L.; Karraker, D. *J. Am. Chem. Soc.* **1977**, *99*, 616. (b) Morelock, M. M.; Good, M. L.; Trefonas, L. M.; Karraker, D.; Maleki, L.; Eichelberger, H. R.; Majeste, R.; Dodge, J. *J. Am. Chem. Soc.* **1979**, *101*, 4858. (c) Morelock, M. M.; Good, M. L.; Trefonas, L. M.; Majeste, R.; Karraker, D. G. *Inorg. Chem.* **1982**, *21*, 3044.
(35) Smith, G.; O'Reilly, E. J.; Kennard, C. H. L. *Aust. J. Chem.* **1983**, *36*, 2175.
(36) Erre, L. S.; Micera, G.; Cariati, F.; Ciani, G.; Sironi, A.; Kozlowski, H.; Baranowski, J. *J. Chem. Soc., Dalton Trans.* **1988**, 363.
(37) Glowiak, T.; Kozlowski, H.; Erre, L. S.; Gulinati, B.; Micera, G.; Pozzi, A.; Bruni, S. *J. Coord. Chem.* **1992**, *25*, 75.
(38) (a) Komson, R. C.; McPhail, A. T.; Mabbs, F. E.; Porter, J. K. *J. Chem. Soc. A* **1971**, 3447. (b) Battaglia, L. P.; Corradi, A. B.; Menabue, L. *Inorg. Chem.* **1983**, *22*, 3251.
(39) Bruce, M. I.; Williams, M. L.; Skelton, B. W.; White, A. H. *J. Chem. Soc., Dalton Trans.* **1983**, 799.
(40) Graf, M.; Stoeckli-Evans, H.; Whitaker, C.; Marioni, P.-A.; Marty, W. *Chimia* **1993**, *47*, 202.
(41) Nishikiori, S. *J. Coord. Chem.* **1996**, *37*, 23.
(42) (a) Pauling, L. *The Nature of the Chemical Bond*; Cornell University Press: Ithaca, NY, 1948. (b) Pimentel, G. C.; McClellan, A. L. *The Hydrogen Bond*; W. H. Freeman: San Francisco, 1960.
(43) Seifer, G. B. *Russ. J. Inorg. Chem.* **1960**, *5*, 33.
(44) Cartraud, P.; Cointot, A.; Renaud, A. *J. Chem. Soc., Faraday Trans.* **1981**, *77*, 1561.

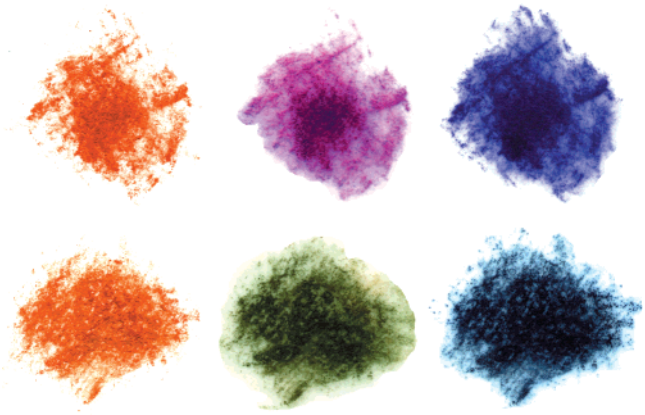

Figure 6. Powder samples of compounds **1** (upper) and **3** (lower) deposited on filter paper and doused with selected solvents: water (as-prepared), tetrahydrofuran, and diethyl ether, from left to right, respectively. The apparent color changes are from orange to red-violet and blue-violet for compound **1**, and from orange to green and blue for compound **3**.

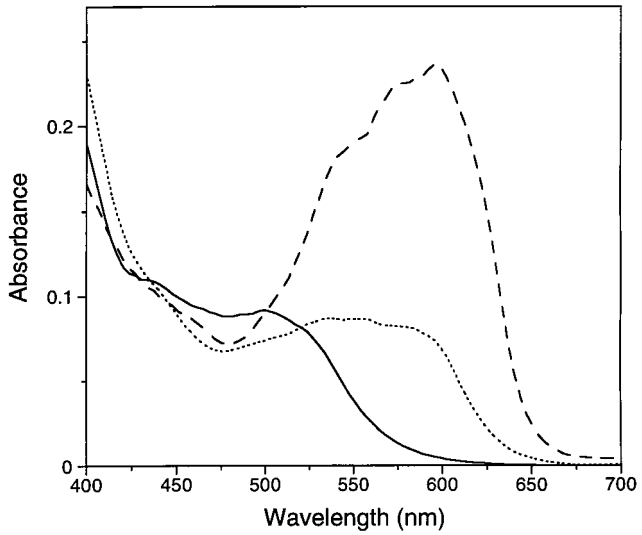

Figure 7. Electronic absorption spectra of compound **1** as-prepared (solid line) and upon exposure to tetrahydrofuran (dotted line) or diethyl ether (dashed line). Units along the vertical axis are arbitrary.

$[Co(H_2O)_2][Re_6S_8(CN)_6]\cdot 2H_2O$ (**2**) or $Cs_2[Co(H_2O)_2]_3[Re_6Se_8(CN)_6]_2\cdot 12H_2O$ is apparent upon exposure to any of the selected solvents.

The diffuse reflectance visible spectra of compounds **1** and **3** before and after solvent exposure were measured to evaluate the absorption features responsible for the color changes. As evident from the spectra displayed in Figures 7 and 8, in both cases the shifts in color are associated with the emergence of an ensemble of new absorption bands situated between 500 and 650 nm. While the wavelengths at which these new bands occur tend to vary only slightly between solvents, large differences in relative intensities are frequently observed. The spectra of the compounds in their initial hydrated forms (solid lines) approximate a superposition of the aqueous solution spectra of Co^{2+} ions and the corresponding $[Re_6Q_8(CN)_6]^{4-}$ cluster. For compound **1**, the peak centered at 434 nm is attributed to an electronic transition within the $[Re_6S_8]^{2+}$ core, based on its presence in the absorption spectra of $[Re_6S_8X_6]^{4-}$ (X = Cl, Br, I) as well as $[Re_6S_8(CN)_6]^{4-}$ clusters.[5,46] In compound **3**, an analogous $[Re_6Se_8]^{2+}$ core transition is centered at 460 nm. The absolute intensities of these peaks do not appear to vary with exposure to solvents; they were therefore chosen as reference peaks for quantitatively comparing intensities of the new absorption bands generated by different solvents. The magnitude of the response of compounds **1** and **3** to a given solvent was estimated from the ratio of the absorbance at 596 and 602 nm (approximately λ_{max} for the most intense of the new bands), respectively, to that of the cluster core transition. The results for some selected solvents are compiled in Tables 3 and 4. On this basis, it is clear that diethyl ether prompts a much greater response than any other solvent tested and that, with a few noteworthy exceptions (discussed further below), the relative ordering of solvent responses follows a similar trend in both compounds. For solvents that do elicit a change, the difference in colors between the compounds is primarily a result of the slightly higher energies of the new absorption features in compound **1** relative to those of compound **3**. Hence, the blue

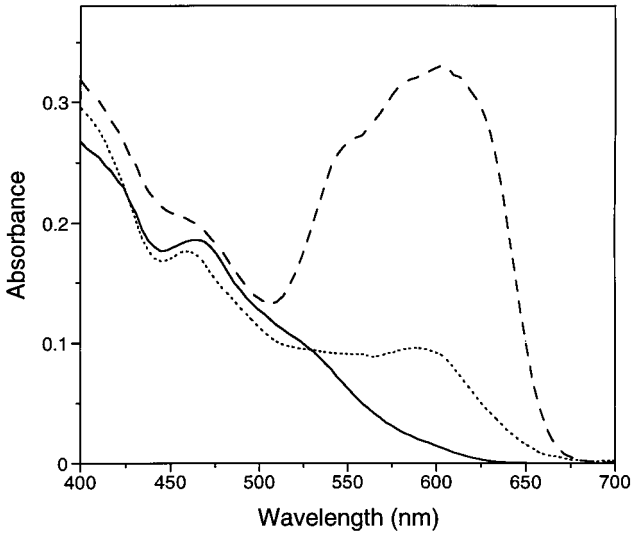

Figure 8. Electronic absorption spectra of compound **3** as-prepared (solid line) and upon exposure to tetrahydrofuran (dotted line) or diethyl ether (dashed line). Units along the vertical axis are arbitrary.

Table 3. Electronic Absorption Data for $[Co_2(H_2O)_4][Re_6S_8(CN)_6]\cdot 10H_2O$ (**1**) upon Exposure to Selected Solvent Vapors

solvent	A_{596}/A_{434}	apparent color
as-prepared (water)	0.053(9)	orange
methanol	0.3(1)	orange
cyclohexane	0.4(1)	orange
acetonitrile	0.4(1)	orange
methyl *tert*-butyl ether	0.40(3)	orange
dichloromethane	0.46(9)	orange
ethanol	0.5(1)	orange-red
dimethylformamide	0.51(6)	orange-red
triethylamine	0.55(7)	orange-red
nitromethane	0.64(3)	red-violet
tetrahydrofuran	0.7(1)	red-violet
acetone	0.8(1)	violet
propionitrile	1.03(3)	violet
n-octanol	1.09(6)	violet
n-propanol	1.61(4)	violet
ethyl acetate	1.7(1)	violet
i-propanol	2.2(4)	blue-violet
diethyl ether	2.3(1)	blue-violet

(45) This reversibility is due to the evaporation of solvent and reabsorption of water from the atmosphere. Subsequent thermogravimetric analyses confirm that the water content matches that in the original samples.

(46) Long, J. R.; McCarty, L. S.; Holm, R. H. *J. Am. Chem. Soc.* **1996**, *118*, 4603.

Table 4. Electronic Absorption Data for $[Co_2(H_2O)_4][Co(H_2O)_3]_4[Re_6Se_8(CN)_6]_3{\cdot}44H_2O$ (**3**) upon Exposure to Selected Solvent Vapors

solvent	A_{602}/A_{460}	apparent color
as-prepared (water)	0.09(2)	orange
cyclohexane	0.12(5)	orange
methanol	0.2(1)	yellow-orange
dichloromethane	0.34(9)	orange
nitromethane	0.46(9)	olive-drab
triethylamine	0.57(8)	brown
acetonitrile	0.6(1)	green
tetrahydrofuran	0.6(1)	green
ethanol	0.7(1)	blue-green
dimethylformamide	0.89(4)	blue-green
acetone	1.00(8)	dark gray
propionitrile	1.11(9)	blue-green
n-octanol	1.17(6)	blue-green
methyl *tert*-butyl ether	1.20(9)	blue-green
ethyl acetate	1.26(4)	blue-green
n-propanol	1.32(4)	blue-green
i-propanol	1.37(3)	blue-green
diethyl ether	1.5(1)	blue

color induced in compound **1** typically has a reddish hue, whereas compound **3** tends toward green.

The spectral features accompanying the color changes in compounds **1** and **3** are fully consistent with the conversion of some or all of their Co^{2+} ions from an octahedral to a tetrahedral coordination geometry. Indeed, the absorption bands that appear are prototypical for tetrahedral Co^{2+} ($e^4t_2^3$) species, which exhibit two characteristic electronic absorptions in the near-infrared and visible regions due to the transitions ν_1 ($^4T_1(F) \leftarrow {}^4A_2$) and ν_2 ($^4T_1(P) \leftarrow {}^4A_2$), respectively. The intensities of these absorptions usually range from 10 to 100 L/(mol·cm) for ν_1 and from 100 to 2000 L/(mol·cm) for ν_2, and they are broadened due to spin−orbit coupling and deviations from ideal tetrahedral symmetry.[47] By comparisons with the electronic absorption spectra of the tetrahedral complexes in $K_2[Co(NCO)_4]$ ($\nu_1 =$ 1200, $\nu_2 =$ 520, 590, and 630 nm)[48] and $Hg[Co(NCS)_4]$ ($\nu_1 =$ 1205, $\nu_2 =$ 599 nm),[49] the new bands between 500 and 650 nm arising from the vapochromic responses of compounds **1** and **3** are assigned to the ν_2 transition of tetrahedrally coordinated Co^{2+} ions. Near-IR spectral measurements on compound **3**, as-synthesized, reveal a very weak absorption centered at 1172 nm, which can be assigned to the $^4T_{2g} \leftarrow {}^4T_{1g}$ transition of the octahedral Co^{2+} ($t_{2g}^5e_g^2$) ions.[47] Upon exposure to diethyl ether, this absorption is replaced by a new band at 1200 nm, which is 10 times greater in intensity and can be ascribed to the ν_1 transition of the now tetrahedral Co^{2+} ions. Unfortunately, the close proximity of the bands in this and other regions of the spectrum precludes any rigorous assessment of the ratio of tetrahedral to octahedral sites for situations in which the conversion might not be complete.

Based on the observed spectral changes, a simple model is proposed to explain the vapochromic behavior of compounds **1** and **3**. The ligand field stabilization energy favors an octahedral over a tetrahedral coordination geometry to a lesser extent for Co^{2+} than for any other transition metal ion.[50] Consequently, its ligand geometry is remarkably sensitive to outer-sphere effects and the nature of any surrounding/coordinating solvent. For example, in solution there exists an equilibrium between octahedral $[Co(NCS)_3L_3]^-$ and tetrahedral $[Co(NCS)_3L]^-$ complexes, such that the octahedral species is heavily favored in water and methanol,[51] while the tetrahedral species is predominant in dimethylformamide and 4-methyl-2-pentanone.[51b,52] This and other evidence[53] combine to suggest that compact solvent ligands capable of deriving support via hydrogen bonding with outer-sphere ligands stabilize an octahedral geometry, while bulkier ligands that cannot do so enforce tetrahedral coordination. Thus, it is proposed that solvent molecules entering the cavities and channels in compounds **1** and **3** displace solvate water molecules, thereby disrupting the hydrogen-bonded network that supports the $[Co_2(H_2O)_4]^{4+}$ clusters (see previous text drawing). Labile water ligands are then released from the destabilized octahedral $Co(NC)_3(H_2O)_3$ centers, leaving a pair of disconnected $Co(NC)_3(L)$ moieties to relax into tetrahedral configurations. The noncyanide ligand (L) could either be a lingering water molecule or a solvent molecule, depending on the coordinating ability and steric requirements of the incoming solvent. The color of the compounds in response to a given solvent is therefore determined by how far to the right it pushes the following equilibrium.

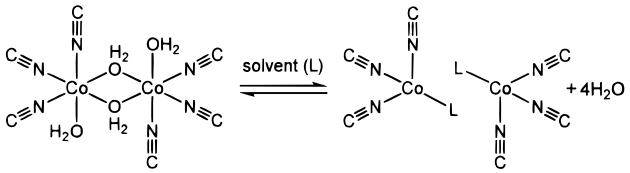

The trends in the vapochromic responses (Tables 3 and 4) of compounds **1** and **3** support the foregoing model. The solubility of a solvent species in water appears to regulate its entry into the water-filled channels and cavities of the solids. Thus, solvents with a solubility in water below ca. 0.5 mol % (such as pentane, benzene, cyclohexane, and dichloromethane) do not cause any significant color change, because they do not enter the pores of the structure. On the other hand, small protic solvents such as methanol can enter the pores, but then do not induce a response owing to their ability to participate in hydrogen bonding (as well as to bridge between metal centers) and maintain the stability of the octahedral Co centers. However, if the steric bulk of a solvent is increased while preserving a similar aptitude for hydrogen bonding at the functional group, then the above equilibrium should shift toward the tetrahedral Co species as the solvent becomes less able to support the bridged Co_2 structure within the close confines of the framework. This trend is confirmed with the vapochromic response along a series of alcohols with increasing steric bulk about the hydroxo functionality: methanol < ethanol < *n*-propanol < *i*-propanol. A similar trend is observed for acetonitrile and propionitrile, species that can act as hydrogen bond acceptors but are unlikely to bridge two metal centers. Molecules of surprisingly long chain length are able to enter the structures, as evidenced by the response (albeit somewhat less immediate) of both compounds to *n*-octanol. Size-selective sensing ability is demonstrated with methyl *tert*-butyl ether (MTBE), which causes a color change in compound **3**, but is apparently too bulky to invade the smaller openings in the framework of compound **1**. Thus, **3** may be useful for the detection of MTBE, a compound that has seen enhanced use in reformulated gasoline

(47) Lever, A. B. P. *Inorganic Electronic Spectroscopy*; Elsevier: Amsterdam, 1968.
(48) Cotton, F. A.; Goodgame, M. *J. Am. Chem. Soc.* **1961**, *83*, 1777.
(49) Cotton, F. A.; Goodgame, D. M. L.; Goodgame, M.; Sacco, A. *J. Am. Chem. Soc.* **1961**, *83*, 4157.
(50) Cotton, F. A.; Wilkinson, G.; Murillo, C. A.; Bochmann, M. *Advanced Inorganic Chemistry*; Wiley: New York, 1999.
(51) (a) Silber, H. B.; Murguia, M. A. *Inorg. Chem.* **1985**, *24*, 3794. (b) Ishiguro, S.; Ozutsumi, K. *Inorg. Chem.* **1990**, *29*, 1117.
(52) Brubaker, C. H.; Johnson, C. E. *J. Am. Chem. Soc.* **1958**, *80*, 5037.
(53) Ishiguro, S. *Bull. Chem. Soc. Jpn.* **1997**, *70*, 1465.

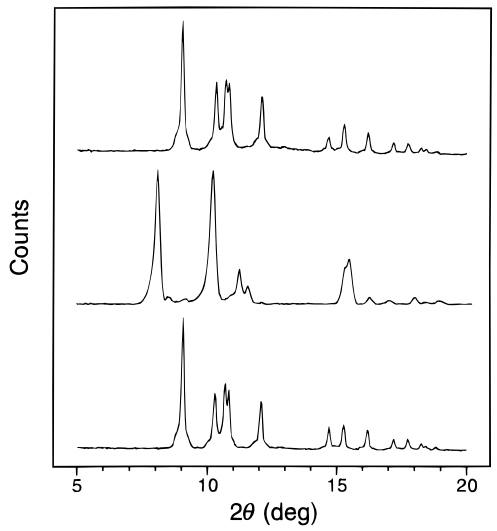

Figure 9. Powder X-ray diffraction data for compound **1** as-prepared (top), upon exposure to diethyl ether (middle), and after allowing the ether to evaporate (bottom). Note that the structural transition caused by interaction with the solvent is reversible.

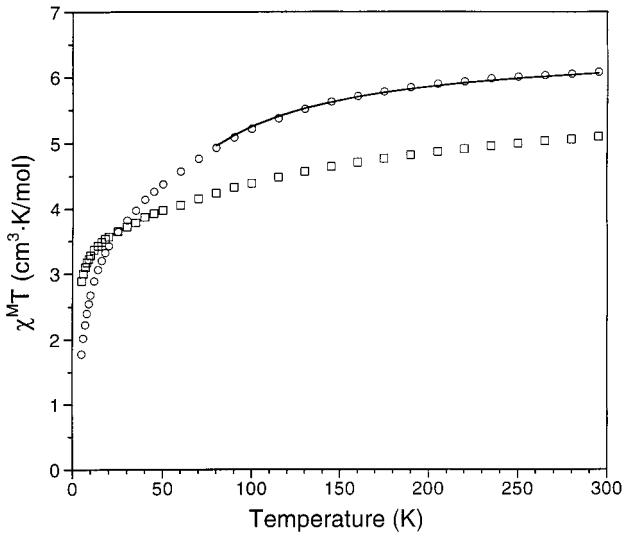

Figure 10. Plot of $\chi^{M}T$ versus temperature for compound **1** as-prepared (circles) and upon exposure to diethyl ether (squares). The solid line represents a fit to the high-temperature data of the as-prepared sample ($\mu_{eff} = 2.828 \cdot (\chi^{M}T)^{1/2}$).

over the last 20 years, and has become an increasingly common pollutant in ambient air and groundwater.[54]

As might be expected, bisection of the Co_2 clusters in the frameworks of compounds **1** and **3** by guest solvent molecules has drastic structural consequences. The changes are easily discernible using powder X-ray diffraction. A portion of the diffraction pattern of hydrated compound **1**, as prepared, is displayed at the top in Figure 9. A sample of this solid was exposed to diethyl ether to give a blue-violet powder, which was then sealed in a capillary and probed by X-ray diffraction. The resulting powder pattern (Figure 9, middle) shows that the solid has completely converted to some new and unknown crystal structure. Upon reexposing the same sample to the atmosphere, the ether quickly evaporated, leaving an orange solid characterized by the diffraction pattern shown at the bottom in Figure 9. The original hydrated crystal structure of the material is fully regained, demonstrating the reversibility of the solvent-induced structural transition. Data collected for compound **3** display wholly analogous behavior. These experiments prove that the vapochromic response to the solvent is associated with a bulk structural change in the material, and is not simply a surface effect. Significantly, in both compounds **1** and **3**, *the three-dimensional connectivity of the framework is not destroyed by removing the bridging water molecules from the crystal structure.* In fact, their removal produces a much more flexible framework, which can swell to accommodate the guest solvent molecules. This flexibility likely accounts for the ability of these compounds to absorb larger molecules than might be expected judging from their hydrated crystal structures.

In contrast to the behavior of compounds **1** and **3**, $Cs_2[Co(H_2O)_2][Re_6S_8(CN)_6]\cdot 2H_2O$ (**2**) and $Cs_2[Co(H_2O)_2]_3[Re_6Se_8(CN)_6]_2\cdot 12H_2O$ display no vapochromic response to any of the selected solvents. Two factors are likely at play here. First, the octahedrally coordinated Co^{2+} ions in these structures are held within a more rigid framework by four cyanide ligands bound in the equatorial plane (see Figure 3). Thus, a tetrahedral coordination geometry cannot be achieved without disrupting the connectivity of the metal−cyanide framework. Note that, for similar reasons, it is not clear if the isolated Co^{2+} sites in compound **3** exhibiting *mer* coordination contribute to its vapochromism (despite the greater flexibility of the dehydrated framework). Second, the frameworks of these compounds are anionic, and the electric fields within the cation-containing cavities should inhibit the displacement of included water by less polar solvent molecules. Indeed, the charge-neutrality of their frameworks is thought to be essential to the vapochromism of compounds **1** and **3**.

Magnetic Behavior. The magnetic susceptibility of compound **1**, both before and after exposure to diethyl ether, was measured over temperatures ranging from 5 to 295 K (see Figure 10). As can be seen in Figures 1 and 2, diamagnetic $[Re_6S_8(CN)_6]^{4-}$ clusters keep the paramagnetic $[Co_2(\mu\text{-}OH)_2]^{4+}$ cluster cores well-separated in the structure of $\mathbf{1}\cdot 2H_2O$. Thus, the monotonic decrease in $\chi^{M}T$ as the temperature of the as-prepared sample is lowered suggests antiferromagnetic coupling between Co^{2+} ions within the dinuclear units, mediated by superexchange through the bridging water molecules. However, a sharpened decline in $\chi^{M}T$ at lower temperatures, most likely due to a combination of the unquenched orbital angular momentum of the Co^{2+} ions and zero-field splitting,[55] complicates interpretation of the data. A least-squares fit of the data between 80 and 250 K to the van Vleck equation (using an exchange Hamiltonian of the form $\hat{H} = -2JS_1\cdot S_2$) gave $J = -5.0$ cm^{-1} and $g = 2.6$ with a 0.39% relative error. The calculated g value is within the range previously observed for octahedrally coordinated Co^{2+} ions.[36] Upon saturation with diethyl ether, the compound exhibits a reduced μ_{eff} of 4.51 μ_B per Co^{2+} ion at 295 K, within the range typically found for tetrahedrally coordinated Co^{2+} ions (3.98 to 4.82 μ_B), and outside that expected for octahedral coordination (4.77 to 5.40 μ_B).[36] The curvature of these data is probably due to spin−orbit coupling.

A Potential Sensing Device. The vapochromic responses of compounds **1** and **3** suggest their possible utility in a simple device capable of detecting solvents of the types listed in the lower portions of Tables 3 and 4. Such a device can be prepared by depositing a thin film of either material onto a glass slide or

(54) Bradley, P. M.; Landmeyer, J. E.; Chapelle, F. H. *Environ. Sci. Technol.* **1999**, *33*, 1877.

(55) (a) Birkelbach, F.; Winter, M.; Flörke, U.; Haupt, H.-J.; Butzlaff, C.; Lengen, M.; Bill, E.; Trautwein, A. X.; Wieghardt, K.; Chaudhuri, P. *Inorg. Chem.* **1994**, *33*, 3990. (b) Mohanta, S.; Nanda, K. K.; Thompson, L. K.; Flörke, U.; Nag, K. *Inorg. Chem.* **1998**, *37*, 1465.

filter paper from a methanol slurry, and only requires a visible spectrophotometric apparatus capable of monitoring two wavelengths simultaneously (e.g., 434 and 596 nm for compound **1** or 460 and 602 nm for compound **3**) in a reflectance geometry. The sensor can then continuously analyze the atmosphere passing over it, and the presence of the volatile organic compound will register with a change in the ratio of the absorbances at the two selected wavelengths.[56] Besides the nature of the response, there are three intrinsic properties of a material that are critical to this type of sensing application: sensitivity, response time, and durability. The sensitivity of the solid combined with its response time determines the lowest concentration of a species that can be detected. The sensitivity of compounds **1** and **3** to diethyl ether was determined to be 40 and 20 ppm, respectively, by exposing a film of each to an atmosphere containing known concentrations of the solvent. The response time is difficult to quantify since it depends on the crystallinity of the solid and the size of the solvent molecules; however, for highly volatile species such as diethyl ether, it is on the order of <1 s. The durability of compound **3** was assessed by measuring absorption spectra before and after 100 cycles of exposing a sample to diethyl ether: no significant change in the spectrum of the orange form of the material was observed.

(56) The sensing ability of just such a device was confirmed for tetrahydrofuran and diethyl ether in a nitrogen flow.

Acknowledgment. This research was funded by the University of California, Berkeley and the University of California Energy Institute. We are grateful to Prof. J. Arnold for use of the thermogravimetric analysis instrument, Prof. D. L. Gin and Prof. A. M. Stacy for access to the X-ray powder diffractometers, Prof. T. D. Tilley for use of the FTIR spectrometer, and Prof. A. M. Stacy for access to the UV−vis spectrophotometer and the SQUID magnetometer. This work was carried out in part at the Stanford Synchrotron Radiation Laboratory, which is operated by the Department of Energy, Office of Basic Energy Sciences.

Supporting Information Available: Figure displaying fit obtained from Rietveld analysis of the X-ray powder diffraction data for compound **2** and tables of crystal data, structure solution and refinement, atomic coordinates, bond lengths and angles, and anisotropic thermal parameters for compounds **1**·$2H_2O$, **2**, and **3** (PDF). An X-ray crystallographic file (CIF). This material is available free of charge via the Internet at http://pubs.acs.org.

JA994186H